

Synthesis, Crystal Structure, and Chromotropic Properties of Mixed-Ligand Nickel(II) Complexes with 1,3-Diketonate and P–N Bidentate Ligands

Machiko Arakawa,[1] Noriyuki Suzuki,[2] Shinobu Kishi,[3] Miki Hasegawa,[3] Keiichi Satoh,[4] Ernst Horn,[5] and Yutaka Fukuda*[1]

[1]Department of Chemistry, Faculty of Science, Ochanomizu University, 2-1-1 Otsuka, Bunkyo-ku, Tokyo 112-8610

[2]RIKEN, Wako 351-0198

[3]Department of Chemistry and Biological Science, College of Science and Engineering, Aoyama Gakuin University, 5-10-1 Fuchinobe, Sagamihara 229-8558

[4]Department of Chemistry, Faculty of Science, Niigata University, 8050 Igarashi-ninomachi, Niigata 950-2181

[5]Department of Chemistry, Faculty of Science, Rikkyo University, 3-34-1 Nishi-Ikebukuro, Toshima-ku, Tokyo 171-8501

Received June 25, 2007; E-mail: fukuda.yutaka@ocha.ac.jp

Mixed-ligand nickel(II) complexes Ni(acac)(dmap)X, [Ni(acac)(dmap)]BPh_4 (**1**), [Ni(acac)(dmap)]BF_4 (**2**), and [Ni(acac)(dmap)NO_3] (**3**) (where acac = acetylacetonate and dmap = 1-dimethylamino-2-diphenylphosphinoethane) have been obtained for the first time and their X-ray single-crystal structures have also been determined. This series of complexes show different structures, hence colors, in the solid state depending on the coordination strength of the anion X^-: the complexes with tetraphenylborate and tetrafluoroborate having no coordination ability are square-planar and orange, while on the contrary, the coordinating nitrate ligand produces an octahedral and pale blue complex. In solution, two types of solvatochromism due to solute–solvent interaction and solute–solute–solvent interaction have been observed and these spectral behaviors are attributed to the changes in their geometries due to the donor/acceptor properties of the solvents. The thermochromic behavior of complex **1** has also been studied with temperature variation UV–vis spectra in various solvents. The behavior of these solvato- and thermo-chromisms of these complexes is due to the intermediate ligand field strength created by the dmap and the acac ligands.

Many of transition-metal complexes show a wide variety of colors due to the d–d transition and CT transition. These colors are sometimes reversibly changed by external stimuli such as light,[1] solvent,[2,3] temperature,[2–5] pressure,[6] and electrons.[7] These chromotropic materials have potential applications including a temperature indicator, an ion sensor, a material detector, etc., and the study of such functional materials has attracted attention in the fields of solution chemistry, structural chemistry, spectrochemistry, and supramolecular chemistry.

It has been our interest to synthesize such chromotropic materials, in particular solvatochromic and thermochromic materials, and we have succeeded in obtaining stable mixed-ligand complexes which show chromotropic behaviors, by carefully selecting suitable combinations of two different chelating ligands, i.e., sterically hindered type and slim type, thereby controlling the coordination environment surrounding the central metal. What was advantageous to us was that the resulting complexes are all very soluble in organic solvents, due to the hydrophobic alkyl substituent groups on the sterically hindered ligands. Therefore, we could observe their chromotropic behavior in various solvents easily and have reported many chromotropic mixed-ligand nickel(II) complexes.[2] The donor set of the chromotropic complexes obtained so far is mostly N_2O_2 such as [Ni(acac)(tmen)]BPh_4 (tmen = *N*,*N*,*N*′,*N*′-tetramethylethylenediamine).[2] Different from the nitrogen donor, the phosphorus donor has a vacant d-orbital and the phosphorus–metal bond is stronger than the nitrogen–metal bond due to the π-back donation. Although soft phosphorus ligands usually make stable complexes with a soft acceptor such as palladium(II) or platinum(II) as explained by the HSAB rule, some complexes with a medium hard acceptor nickel(II) have been also reported.[8,9] It is of interest to understand the formation and structure of new nickel(II) mixed-ligand complexes containing phosphorus donor instead of nitrogen donor. As reported previously, the mixed-ligand complex [Ni(acac)(dppe)]BF_4 containing 1,2-bis(diphenylphosphino)ethane (dppe) as a diphosphine bidentate ligand, keeps its stable square-planar structure even in strong donor solvents without showing any solvatochromic properties.[10] In this paper, we replaced dppe with a P–N bidentate ligand, 1-dimethylamino-2-diphenylphosphinoehtane (dmap, Fig. 1), and obtained the following new chromotropic complexes: [Ni(acac)(dmap)]BPh_4 (**1**), [Ni(acac)(dmap)]BF_4 (**2**), and [Ni(acac)(dmap)NO_3] (**3**). The crystal structures have been determined by single-crystal X-ray analysis. The solution behaviors of the complexes obtained were investigated by UV–vis spectroscopy, NMR spec-

Published on the web January 10, 2008; doi:10.1246/bcsj.81.127

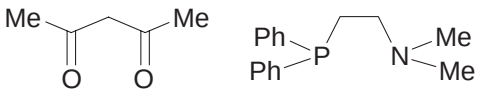

Hacac dmap

Fig. 1. Hacac ligand and P–N bidentate ligand dmap.

Table 1. Donor Numbers (DN) and Acceptor Numbers (AN) Used in This Report

Solvent	Abbreviation	DN	AN
1,2-Dichloroethane	DCE	0	17
Nitromethane	NM	2.7	21
Benzonitrile	BzCN	12	16
Acetonitrile	ACN	14	19
Tetramethylenesulfoxide	TMS	15	19
Acetone	ACO	17	13
Ethanol	EtOH	20	38
n-Butanol	BuOH	22	37
N,*N*-Dimethylformamide	DMF	27	16
Dimethylsulfoxide	DMSO	30	19
Pyridine	PY	33	14

troscopy, and molar conductivity measurements. Using UV–vis spectra of complex **2** in different donor solvents at different temperatures, the $\ln K$, ΔH°, and ΔS° values for equilibrium between the square-planar and octahedral species have been determined. These results were compared with those previously reported for the diamine and diphosphine derivatives, i.e., the Ni(acac)(diamine)X and Ni(acac)(diphosphine)X analogs.[2,10]

Experimental

Materials. Starting materials for synthesizing the dmap, and metal salts and 1,3-diketonates were commercially available and were used without further purification. "Spectro-grade" solvents were used for spectral measurements. The abbreviation of the solvents with donor numbers (DN) and acceptor numbers (AN) are listed in Table 1.[11]

Physical Measurements. Elemental analyses (C, H, and N) were measured on a Perkin-Elmer 2400 II CHN analyzer. IR spectra were obtained as KBr pellets on a Perkin-Elmer FT-IR SPECTRUM 2000. Mass spectra were obtained on a JEOL JMS-700 Mstation in the Fast Atom Bombardment (FAB) mode using PEG-600 as standard and 2-nitrophenyl octyl ether (NPOE) as matrix. Magnetic data were measured on a Shimadzu Torsion Magnetometer MB-100 at room temperature and the effective magnetic moments (μ_{eff}) were calculated with correcting Pascal's constants.[12] NMR spectra were obtained on a JEOL JNM-AL400 and referenced to PPh_3 (δ −6.00) for the ^{31}P nucleus. Electric conductance of the solution was measured with a Conductivity Outfit Model AOC-10 (Denki-Kagaku-Keiki Co., Ltd.) at 25 ± 0.1 °C. UV–vis spectra were obtained on a UV-3100PC Shimadzu Spectrophotometer using a 1 cm quartz cell. Temperature variation spectra were measured on UV-3101PC Shimadzu Spectrophotometer and Shimadzu TCC-260 temperature controller using 1 cm glass cell which was sealed under argon gas.

Synthesis of dmap. 1-Dimethylamino-2-diphenylphosphinoethane (dmap) was prepared under N_2 and dehydration condition by the literature[13] method with a slight modification. To a solution of PPh_2H (0.389 g, 2.09 mmol) in tetrahydrofuran (65 mL), *tert*-BuOK (0.562 g, 5.01 mmol) was added, upon which the color changed to orange. After stirring for fifteen minutes at room temperature, $Me_2NCH_2CH_2Cl\cdot HCl$ (0.361 g, 2.51 mmol) was added to the solution and refluxed at 75 °C for 6 h. The orange suspension became white as the reaction proceeded. Solvent was removed in vacuo and the reaction was stopped by adding an aqueous saturated NH_4Cl. The mixture was extracted with diethyl ether (20 mL × 3) and dried with $MgSO_4$. After removing the solvent, yellow-brown oil was obtained. Yield 60–76%. $^{31}P\{^1H\}$ NMR ($CDCl_3$): δ −20.75 (s). ^1H NMR ($CDCl_3$): δ 7.43–7.30 (m, aromatic 10H), 2.41–2.37 (t, methylene 2H), 2.26–2.22 (m, methylene 2H and methyl 6H).

Synthesis of [Ni(acac)(dmap)]BPh_4 (1). The complex was prepared by the literature method.[9] dmap (0.257 g, 1 mmol) in diethyl ether (ca. 5 mL) was added to an ethanol solution (50 mL) of $[Ni(acac)_2(H_2O)_2]$ (0.293 g, 1 mmol), followed by the addition of $NaBPh_4$ (0.513 g, 1.5 mmol) in ethanol (10 mL), and the orange product precipitated. This was recrystallized from a acetone–ethanol mixture (1:1). Yield 62%. Orange. Anal. Found: C, 73.54; H, 6.52; N, 1.87%. Calcd for $C_{45}H_{47}NBNiO_2P$: C, 73.60; H, 6.45; N, 1.91%. $^{31}P\{^1H\}$ NMR (CD_3NO_2): δ 28.81 (s). ^1H NMR (CD_3NO_2): δ 8.06–7.60 (m, aromatic 10H in dmap), 7.34–6.82 (m, aromatic 20H in BPh_4^-), 5.68 (s, methine 1H in acac), 2.59 (br, 10H in dmap), 2.01 (s, methyl 6H in acac). Solid reflection $\lambda_{\max}$ (nm): 464. Selected IR bands (cm^{-1}): $\nu_{C=O} + \nu_{C=C}$ 1565, 1527 ($\Delta_{\text{acac}} = 38\,cm^{-1}$). FAB^+ MS: 415, $M^+ - BPh_4$. Diamagnetic.

Synthesis of [Ni(acac)(dmap)]BF_4 (2). Hacac (0.100 g, 1 mmol), Et_3N (0.101 g, 1 mmol), and dmap (0.257 g, 1 mmol) in diethyl ether (ca. 5 mL) were added in this order to a 20 mL of ethanol solution of $Ni(BF_4)_2\cdot 6H_2O$ (0.340 g, 1 mmol) in an ice bath. After stirring the deep red solution for 20 min, orange crystals were obtained. Vapor diffusion of diethyl ether into the acetone solution gave orange single crystals suitable for X-ray analysis. Yield 53%. Orange. Anal. Found: C, 49.76; H, 5.51; N, 2.69%. Calcd for $C_{21}H_{27}NBF_4NiO_2P$: C, 50.25; H, 5.42; N, 2.79%. $^{31}P\{^1H\}$ NMR (CD_3NO_2): δ 29.51 (s). ^1H NMR (CD_3NO_2): δ 8.06–7.62 (m, aromatic 10H in dmap), 5.69 (s, methine 1H in acac), 2.60 (br, 10H in dmap), 2.06 (s, methyl 6H in acac). Solid reflection $\lambda_{\max}$ (nm): 463. Selected IR bands (cm^{-1}): $\nu_{C=O} + \nu_{C=C}$ 1575, 1530 ($\Delta_{\text{acac}} = 45\,cm^{-1}$). FAB^+ MS: 415, $M^+ - BF_4$. Diamagnetic.

Synthesis of [Ni(acac)(dmap)NO_3] (3). This complex was prepared by the same method used for complex **2**, but starting from $Ni(NO_3)_2\cdot 6H_2O$. Yield 51%. Pale blue. Anal. Found: C, 52.25; H, 5.80; N, 5.70%. Calcd for $C_{21}H_{27}N_2NiO_5P$: C, 52.87; H, 5.70; N, 5.87%. Solid reflection $\lambda_{\max}$ (nm): 971, 609. Selected IR bands (cm^{-1}): $\nu_{C=O} + \nu_{C=C}$ 1593, 1519 ($\Delta_{\text{acac}} = 74\,cm^{-1}$); combination bands of bidentate NO_3 1764, 1718 ($\Delta_{NO_3} = 46\,cm^{-1}$). FAB^+ MS: 415, $M^+ - NO_3$. μ_{eff} (BM): 3.22.

X-ray Crystallography. X-ray data of complex **1** was collected on a Rigaku RAXIS CS imaging plate area detector with graphite-monochromatized Mo Kα radiation ($\lambda = 0.71073$ Å) at 100 K. A total of 88 oscillation images were collected, and the intensities were corrected for Lorentz and polarization effects. The structure was solved by heavy-atom Patterson methods[14] and expanded using Fourier techniques.[15] The unit cell contains two crystallographically independent molecules which have almost same structure. All non-hydrogen atoms were refined with anisotropic thermal parameters. Hydrogen atoms were included in calculated positions and refined with isotropic thermal parameters. All calculations were performed using the CrystalStructure[16] crystallographic software package except for refinement, which

Table 2. Crystallographic Data

	1	**2**	**3**	[Ni(acac)(tmen)]BPh_4
Crystal color	orange	orange	blue	red
Empirical formula	$C_{45}H_{47}BNNiO_2P$	$C_{21}H_{27}BF_4NNiO_2P$	$C_{21}H_{27}N_2NiO_5P$	$C_{35}H_{43}BN_2NiO_2$
Formula weight	734.36	501.94	477.13	593.26
Crystal dimensions/mm^3	$0.60 \times 0.40 \times 0.30$	$0.55 \times 0.50 \times 0.30$	$0.29 \times 0.15 \times 0.10$	$0.50 \times 0.20 \times 0.20$
Crystal system	triclinic	monoclinic	monoclinic	monoclinic
Space group	$P\bar{1}$	$P2_1/c$	$P2_1/c$	$P2_1/c$
a/Å	9.7805(12)	14.71(2)	16.667(2)	16.855(4)
b/Å	21.554(3)	12.243(11)	7.9761(7)	12.111(4)
c/Å	21.618(4)	14.87(2)	17.251(2)	18.324(9)
α/°	119.337(4)	90	90	90
β/°	99.184(4)	116.20(7)	91.260(2)	122.10(5)
γ/°	94.174(4)	90	90	90
V/Å^3	3861.0(10)	2403(4)	2292.7(4)	3169(2)
Z	4	4	4	4
D_{calcd}/Mg m^{-3}	1.263	1.387	1.382	1.244
μ/mm^{-1}	0.5821	0.921	0.949	0.645
θ_{max}/°	27.50	27.50	28.46	27.50
No. of observations	17046	5304	3659	5634
Parameters	921	389	352	543
R_1 ($I > 2\sigma$)	0.0563	0.0516	0.0602	0.0645
R_w	0.1367	0.1556	0.0605	0.1733
S	1.037 (Fit on F^2)	1.060 (Fit on F^2)	0.224 (Fit on F)	1.083 (Fit on F^2)

was performed using full-matrix least-square techniques SHELXS-97.[17]

X-ray data of complex **2** and [Ni(acac)(tmen)]BPh_4 as the reference data were collected on a Mac Science M03XHF four-circle diffractometer with graphite-monochromatized Mo Kα radiation ($\lambda = 0.71073$ Å) at 298 K. The unit cell parameters were determined by a least-square method of 22 reflections ($31.54° < 2\theta < 35.00°$ for complex **2**, $10.33° < 2\theta < 23.54°$ for [Ni(acac)(tmen)]BPh_4). A semi-empirical absorption correction was applied using psi-scans. The intensity data were collected by the $\omega - 2\theta$ scan technique and the intensities were corrected for Lorentz and polarization effects. The structure was solved by the direct method SIR92,[18] and were refined by full-matrix least-square techniques SHELXS-97.[17] All non-hydrogen atoms were refined with anisotropic thermal parameters. Hydrogen atoms were included in calculated positions and refined with isotropic thermal parameters. All diagrams and calculations were performed using maXus (Bruker Nonius, Delft & MacScience, Japan).

X-ray data of complex **3** was collected on a Bruker Smart APEX CCD diffractometer with graphite-monochromatized Mo Kα radiation ($\lambda = 0.71073$ Å) at 296 K. The unit cell parameters were determined by a least-square method of 3348 reflections ($4.719° < 2\theta < 47.325°$). The intensity data were collected by the $\omega - 2\theta$ scan technique, the intensities were corrected for Lorentz and polarization effects, and an absorption correction was applied using SADABS.[19] The structure was solved by the direct method SIR92,[18] and expanded using Fourier techniques.[15] All non-hydrogen atoms were refined with anisotropic thermal parameters. Hydrogen atoms were included in calculated positions and refined with isotropic thermal parameters. All calculations were performed using the teXsan[20] crystallographic software package of Molecular Structure Corporation.

Crystallographic data and refinement parameters are listed in Table 2. Crystal data have been submitted to CCDC; the document numbers are 287901 (**1**), 288106 (**2**), 662907 (**3**), and 662908 ([Ni(acac)(tmen)]BPh_4). Copies of this information may be obtained free of charge via www.ccdc.cam.ac.uk/data_request/cif, by e-mailing: data_request@ccdc.cam.ac.uk, or contacting CCDC, 12, Union Road, Cambridge, CB2 1EZ, UK [Fax: +44 1223 336033].

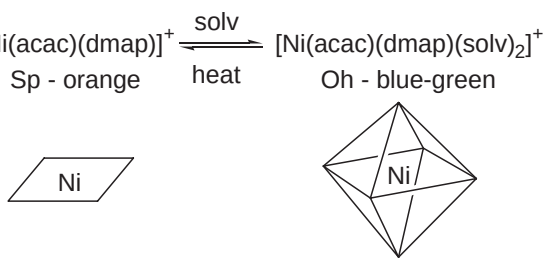

Scheme 1. Equilibrium between square-planar (Sp) and octahedral (Oh) structure for complex **1** and **2**.

Equilibrium Constants. For solvatochromic and thermochromic behavior of the complex **2**, a quantitative approach was performed with $\ln K$, $\Delta H°$, and $\Delta S°$ values for Scheme 1. Temperature-variation UV–vis spectra were measured in four donor solvents, ACN, ACO, EtOH, and BuOH, in which two structures (Sp and Oh) coexisted at room temperature. In ACN solution, there are three absorptions; the band at 465 nm attributes to the square-planar structure and the weak bands at 600 and 945 nm attribute to the octahedral structure. As the temperature decreased, the intensity at 465 nm decreased, while the intensity of other bands increased with the isosbestic point. Since the ε_{Oh} at 465 nm is much smaller than ε_{Sp}, the equilibrium constant of Scheme 1 is given by the Eq. 1 where $A_{Sp}{}^o$ is the absorbance in 100% of the square-planar structure and A_{Sp} is the absorbance measured at any temperature.

$$K = [Oh]/[Sp] = (A_{Sp}{}^o - A_{Sp})/A_{Sp}. \quad (1)$$

In the linear $\ln K - 1/T$ plot, $\Delta H°$ and $\Delta S°$ values were calculated from the slope and intercept, respectively.[5]

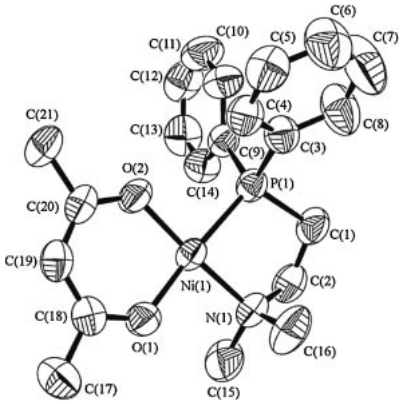

Fig. 2. An ORTEP drawing of [Ni(acac)(dmap)]BF_4 (**2**). The BF_4^- ion is not shown for clarity. Displacement ellipsoids are drawn with 50% probability.

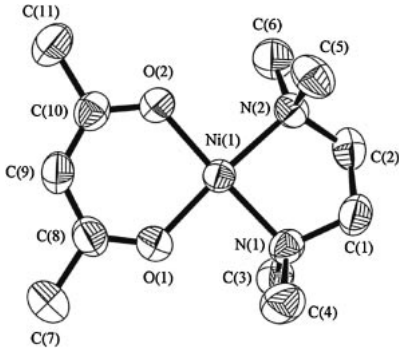

Fig. 3. An ORTEP drawing of [Ni(acac)(tmen)]BPh_4. The BPh_4^- ion is not shown for clarity. Displacement ellipsoids are drawn with 50% probability.

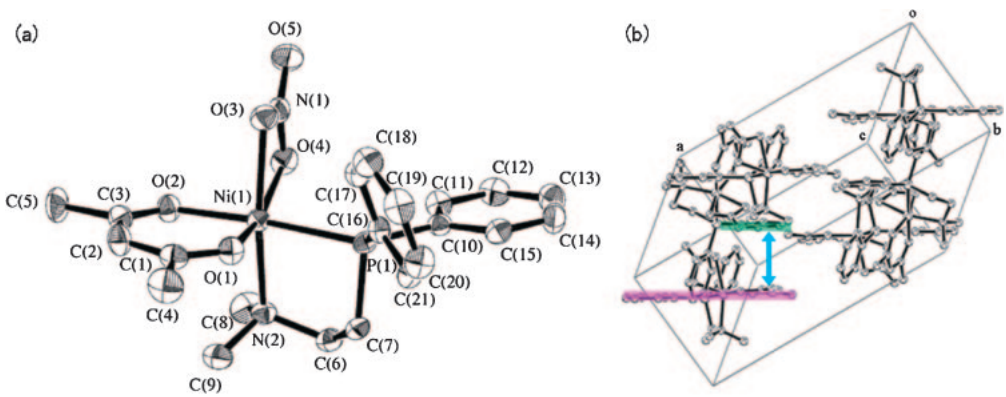

Fig. 4. Molecular (a) and packing (b) structures of [Ni(acac)(dmap)(NO_3)] (**3**). Displacement ellipsoids are drawn with 30% probability. There is a π-stuck interaction between two planes: Ni–acac–Ph (pink) and Ph (green).

Results and Discussion

Properties of the Complexes in Solid State and Their Crystal Structures. Complexes **1** and **2** are diamagnetic and have one strong band at 464 nm in the solid-state reflectance spectra, which indicate that they have a square-planar structure of Ni^{2+}: d^8 electron metal.[21] On the other hand, complex **3** is paramagnetic ($\mu_{eff} = 3.22$ BM) and has two bands at around 971 and 609 nm in the solid-state reflectance spectrum, hence it has an octahedral structure. In the IR spectra, there are weak but important bands due to the coordination mode of NO_3^- in region of 1700–1800 cm^{-1}, where one band appears due to the free NO_3^- ion. This band splits into two on coordination; when the splitting is small ($\Delta_{NO_3} = 20 - 25\ cm^{-1}$) the NO_3^- is a monodentate, but when it is larger than 25 cm^{-1}, the NO_3^- is a bidentate.[22] In complex **3**, there are two bands ($\Delta_{NO_3} = 46\ cm^{-1}$), indicating that the NO_3^- is a bidentate.

It is interesting to note that the differences between $\nu_{C=O}$ and $\nu_{C=C}$ of acac ligand (Δ_{acac}) are also characteristic.[2,21–24] This difference varies greatly from a square-planar structure to an octahedral one. As the Ni–O(acac) bonds become weaker, the C=O bonds become stronger and the C=C bonds become weaker, therefore Δ_{acac} value increases. We could confirm their structures from this viewpoint: the Δ_{acac} observed in the octahedral complex **3** is larger than those of the square-planar complexes **1** and **2**.

Figures 2, 3, and 4 show the molecular structures of complex **2**, [Ni(acac)(tmen)]BPh_4, and complex **3**, respectively. The selected bond lengths and angles are listed in Table 3. For complex **2**, the central Ni^{II} is coordinated by two oxygen atoms of the acac ligand, and one phosphorus and one nitrogen of the dmap ligand to give a four-coordinated square-planar structure. The two Ni–O(acac) bond lengths are different; the Ni–O(trans to P) distance is longer than the Ni–O(trans to N) distance because of the stronger trans influence originated by the phosphorus atom. The former is comparable to the corresponding Ni–O(acac) distances found in [Ni(acac)(dppe)]-BF_4.[10] Similarly, the latter is comparable to those in [Ni(acac)-(tmen)]BPh_4. The bite angle of dmap ligand in complex **2**, P–Ni–N = 87.60(10)°, lies between the values of dppe in [Ni(acac)(dppe)]BF_4, P–Ni–P = 86.87(4)°, and tmen in [Ni-(acac)(tmen)]BPh_4, N–Ni–N = 87.97(11)°. From these results, the dmap complex is expected to have an intermediate ligand field strength of the dppe complex and the tmen complex. This is supported by solution behavior given later. Complex **1** also shows a similar structural property to complex **2**.

As stated above, the octahedral structure of complex **3** was confirmed by crystallographic analysis. The small bite angle of NO_3 results in a distorted structure; O(1)–Ni(1)–O(4) = 163.1(2)° and N(2)–Ni(1)–O(3) = 161.2(2)°. The Ni–O(acac) and Ni–O(NO_3) bond lengths are similar to those previously reported for the diamine analogues,[23] which indicates that

Table 3. Selected Bond Lengths (Å) and Angles (°)

1[a]			
Ni(1)–O(1)	1.8790(17)	O(1)–Ni(1)–O(2)	96.03(9)
Ni(1)–O(2)	1.842(2)	P(1)–Ni(1)–N(1)	87.78(6)
Ni(1)–P(1)	2.1617(7)	O(1)–Ni(1)–N(1)	89.08(9)
Ni(1)–N(1)	1.969(3)	O(1)–Ni(1)–P(1)	175.79(8)
O(1)–C(18)	1.286(3)	O(2)–Ni(1)–N(1)	174.84(9)
O(2)–C(20)	1.298(4)	O(2)–Ni(1)–P(1)	87.15(6)
C(18)–C(19)	1.393(5)		
C(19)–C(20)	1.381(3)		
2			
Ni(1)–O(1)	1.866(3)	O(1)–Ni(1)–O(2)	95.10(11)
Ni(1)–O(2)	1.837(2)	P(1)–Ni(1)–N(1)	87.60(10)
Ni(1)–P(1)	2.161(3)	O(1)–Ni(1)–N(1)	89.51(11)
Ni(1)–N(1)	1.960(2)	O(1)–Ni(1)–P(1)	173.68(7)
O(1)–C(18)	1.271(3)	O(2)–Ni(1)–N(1)	175.04(9)
O(2)–C(20)	1.297(3)	O(2)–Ni(1)–P(1)	87.99(9)
C(18)–C(19)	1.382(4)		
C(19)–C(20)	1.370(5)		
[Ni(acac)(tmen)]BPh_4			
Ni(1)–O(1)	1.840(2)	O(1)–Ni(1)–O(2)	94.67(10)
Ni(1)–O(2)	1.847(2)	N(1)–Ni(1)–N(2)	87.97(11)
Ni(1)–N(1)	1.937(3)	O(1)–Ni(1)–N(1)	87.71(11)
Ni(1)–N(2)	1.946(3)	O(1)–Ni(1)–N(2)	175.39(11)
O(1)–C(8)	1.265(4)	O(2)–Ni(1)–N(1)	177.41(10)
O(2)–C(10)	1.276(4)	O(2)–Ni(1)–N(2)	89.68(11)
C(8)–C(9)	1.388(5)		
C(9)–C(10)	1.367(5)		
3			
Ni(1)–O(1)	1.976(4)	O(1)–Ni(1)–O(2)	91.9(2)
Ni(1)–O(2)	1.986(4)	P(1)–Ni(1)–N(2)	85.1(1)
Ni(1)–P(1)	2.426(1)	O(3)–Ni(1)–O(4)	59.8(2)
Ni(1)–N(2)	2.142(4)	O(1)–Ni(1)–O(4)	163.1(2)
O(1)–C(1)	1.263(7)	O(2)–Ni(1)–P(1)	175.3(1)
O(2)–C(3)	1.247(7)	O(3)–Ni(1)–N(2)	161.2(2)
C(1)–C(2)	1.396(8)		
C(2)–C(3)	1.400(8)		
Ni(1)–O(3)	2.168(4)		
Ni(1)–O(4)	2.126(4)		

a) Only the data for one of two independent molecules are shown.

the trans influence of the phosphorus donor is not obvious in this octahedral structure. It is interesting that one phenyl ring of dmap (C(10)–C(15)) is coplanar to the Ni–acac ring within the molecule (pink plane in Fig. 4b), and the other phenyl ring of dmap (C(16)–C(21), green plane in Fig. 4b) forms a π-stack with an adjacent Ni–acac ring (shortest distance C(3)–C(20) = 3.635 Å). The Ni–O(acac), Ni–P, and Ni–N distances in the six-coordinated complex **3** are respectively longer than those in the four-coordinated complexes **1** and **2**, in accordance with the first bond variation rule.[11]

Solvato- and Thermochromism of the Complexes in Solution. All complexes showed solvatochromism and thermochromism. The "solute–solvent interaction" operates in the case of complexes **1** and **2**, while the "solute–solute–solvent interaction" operates in the case of complex **3**. In Table 4, spectral data for these complexes in various solvents with different donor number are summarized. Complex **1** showed a solvatochromic behavior similar to that of complex **2**, even though its behaviors in EtOH and BuOH could not be measured because complex **1** is not soluble in these solvents. Figure 5 shows the UV–vis spectra and color variations of complex **2** in DCE, ACN, and DMSO. In DCE, the solution is orange, and the spectrum shows a strong absorption band at 463 nm ($\varepsilon = 560\,\mathrm{dm^3\,mol^{-1}\,cm^{-1}}$), which means that the complex **2** has a square-planar stereochemistry according to the shift of the equilibrium shown in Scheme 1 to the left side. On the other hand, the solution is blue-green in the strong donor, DMSO, showing two relatively weak bands at 1059 and 643 nm ($\varepsilon = 13.2$ and $7.50\,\mathrm{dm^3\,mol^{-1}\,cm^{-1}}$, respectively). This means that two DMSO molecules are bound to the Ni^{2+} center to form an octahedral geometry due to the shift of the equilibrium in Scheme 1 to the right. In solvent with a medium donor strength, such as ACN, the spectrum shows a strong band at 465 nm and a relatively weak band around 950 nm, indicating that both square-planar and octahedral species coexist in solution and the equilibrium position depends on the temperature. The spectrum of complex **2** in ACN shows only one band attributable to the octahedral species because the other band near 600 nm seems to be hidden in a strong band attributed to the square-planar species. This is supported by the spectrum in the same N-donor pyridine whose λ_{max} are 971 and 588 nm. The temperature-variation spectra shown in Fig. 8 also agree with a shift of the equilibrium in Scheme 1 (see in thermochromic section). The $\ln K$ values given by Eq. 1 vs. DN at room temperature (300 K) are plotted in Fig. 6. It shows that the equilibrium in Scheme 1 shifts to the right (octahedral structure) as the DN of the solvent increases. The major species in ACO is a square-planar structure for complex **2**, while both square-planar and octahedral species exist in ACO with each species given at a comparable concentration in the case of the tmen analog, [Ni(acac)(tmen)]BPh_4.[2] These indicate that the square-planar species is much more stable in the dmap complex **2** due to the strong phosphorus donor and the higher steric hindrance at axial site of Ni^{2+} in comparison with the tmen complex. As already reported, the corresponding dppe complex has very strong ligand field strength, therefore only the square-planar species are observed in strong donor solvents without any solvatochromic behavior.[10]

In some solvents such as ACN and EtOH, complex **2** exists in two forms at room temperature, and the equilibrium in Scheme 1 shifts depending on the temperature: the solution turns orange at high temperature and green at low temperature. The temperature-variation UV–vis spectra in four solvents (ACN, ACO, EtOH, and BuOH) were measured in the concentration range 0.0019–0.0021 $\mathrm{mol\cdot dm^{-3}}$, as exemplified in Fig. 7a. As the temperature decreases, the absorbance at 465 nm corresponding to the square-planar species decreases, and that at 600 nm corresponding to the octahedral species increases at the same time. The $\ln K$ is plotted versus the inverse of temperature (see Fig. 7b). The ΔH° and ΔS° values were calculated from the slope and intercept of the plot (see Table 5 and Fig. 8). For determining the solvent donor ability, the

Table 4. λ_{max} (nm) and ε ($dm^3 mol^{-1} cm^{-1}$) in Parenthesis for Complexes in Various Solvents with Different Donor Number[a)]

Complex	DCE	NM	BzCN	ACN	TMS	ACO	EtOH	BuOH	DMF	DMSO	PY
1	462 (491)	463 (444)	464 (294)	462 (237)	462 (219)	463 (446)	—	—			
			600[b)]	600[b)]	630[b)]				623 (10.4)	636 (8.05)	587 (9.50)
			950 (14.7)[c)]	942 (15.9)	1050 (3.43)[c)]				1030 (18.7)	1059 (14.4)	975 (7.71)
2	463 (560)	463 (414)	465 (316)	465 (217)	462 (203)	464 (435)	462 (183)	462 (94.3)			
			600[b)]	600[b)]	630[b)]		650 (5.21)	636 (5.58)	621 (10.7)	643 (7.50)	588 (9.00)
			950 (7.77)[c)]	945 (13.2)	1070 (2.98)[c)]		1056 (4.93)	1046 (7.22)	1032 (18.8)	1059 (13.2)	971 (7.29)
3	460[b)]	463 (213)	460[b)]	463 (65.9)	461 (164)	460[b)]	462 (116)	461 (63.5)			
	603 (26.4)	600[b)]	604 (21.8)	601 (20.4)	600[b)]	604 (24.7)	605 (9.14)	607 (13.0)	623 (9.66)	650 (7.24)	587 (10.0)
	1008 (24.9)	1001 (12.7)	1003 (20.7)	1004 (20.2)	1017 (7.79)	1010 (24.9)	1022 (9.91)	1021 (13.8)	1025 (16.7)	1068 (12.5)	956 (7.24)

a) Concentration of the complex is 0.00525 mol dm^{-3}. b) Shoulder. c) Broad.

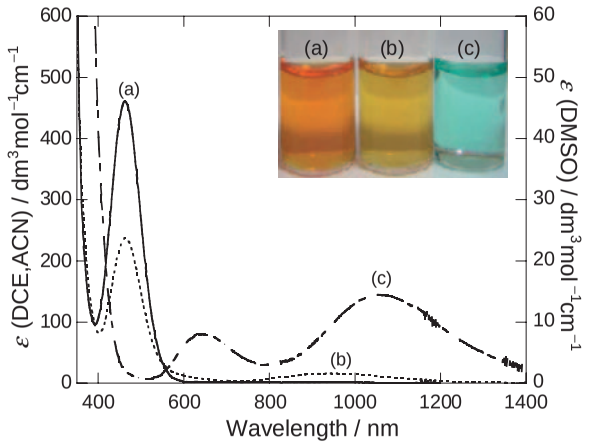

Fig. 5. UV–vis spectra of [Ni(acac)(dmap)]BF_4 (**2**); (a) DCE, (b) ACN, and (c) DMSO.

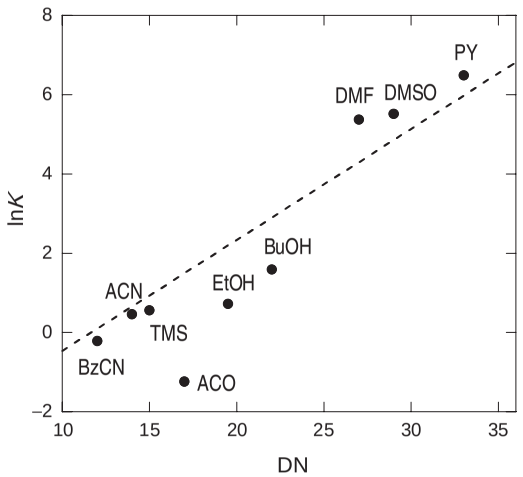

Fig. 6. ln K–DN plot at 300 K of [Ni(acac)(dmap)]BF_4 (**2**). The solvents used are listed in Table 1.

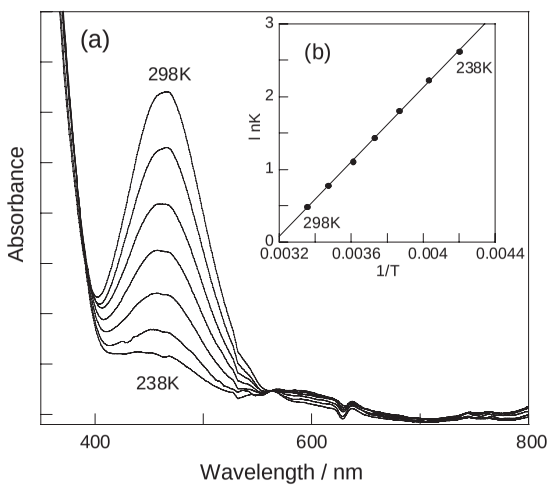

Fig. 7. (a) Temperature-dependence spectra of [Ni(acac)-(dmap)]BF_4 (**2**) in ACN. Temperatures are 298, 287, 277, 268, 258, 248, and 238 K starting from the top. The peaks at 540 and 650 nm are due to noise from the apparatus. (b) ln K–1/T plot.

Table 5. Equilibrium Constants at 300 K, Enthalpies ($kJ\,mol^{-1}$) and Entropies ($J\,mol^{-1}\,K^{-1}$)

Solvent	K	ΔH^o	ΔS^o
ACN	1.587	−21.25	−67.35
ACO	0.2898	−22.64	−103.3
EtOH	2.064	−24.02	−69.29
BuOH	4.944	−24.32	−77.21

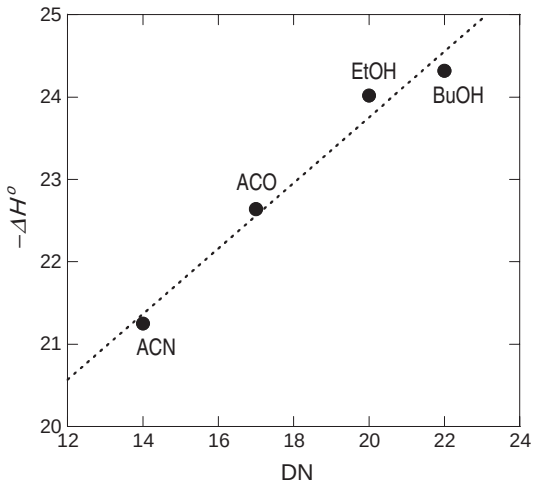

Fig. 8. $-\Delta H^o$–DN plot of [Ni(acac)(dmap)]BF_4 (**2**).

definition of the Gutmann's donor number (DN) is the $-\Delta H^o$ value of an addition reaction in which a donor such as solvent coordinates to the trigonal-bipyramidal $SbCl_5$ changing to an octahedral geometry.[2] The same tendency was observed in $-\Delta H^o$ versus DN plot obtained in this work. Furthermore, the K value determined for ACO solution at 298 K is less than that expected from its DN in Fig. 6, which is due to large contribution of a negative ΔS^o value. It is considered that at room temperature, an acetone molecule is difficult to coordinate to the complex because of its medium donor ability and the steric hindrance of two methyl groups compared with the other three solvents, but at low temperature, the rotation of methyl groups is decreased and the partial negative charge of oxygen atom is strengthened by intermolecular interaction, hence, the acetone molecule coordinates to the complex more easily.

The solvatochromism of complex **3** depends not only on the donor property, but also on the acceptor property of the solvent. In the strong acceptor solvent, the weak donor NO_3^- easily dissociates and is solvated by the solvent. In the strong donor solvent, coordination of the solvent and NO_3^- to the metal ion compete with each other. The structures of complex **3** in various solvents were investigated by UV–vis spectroscopy (Table 4 and Fig. 9) and molar conductivity measurements (Table 6). In DCE, the UV–vis spectrum has two weak bands indicating an octahedral structure and the molar conductivity is much lower than that of the 1:1 electrolyte. This means that the complex preserves an octahedral structure with the NO_3^- ion coordinated (Oh_1 structure) in DCE. In solvents with strong acceptor ability, such as NM, the molar conductivity indicates that about 30 percent of the complex dissolved undergoes NO_3^- dissociation. In the UV–vis spectrum of the NM solution, one strong absorption band appears at 463 nm, while

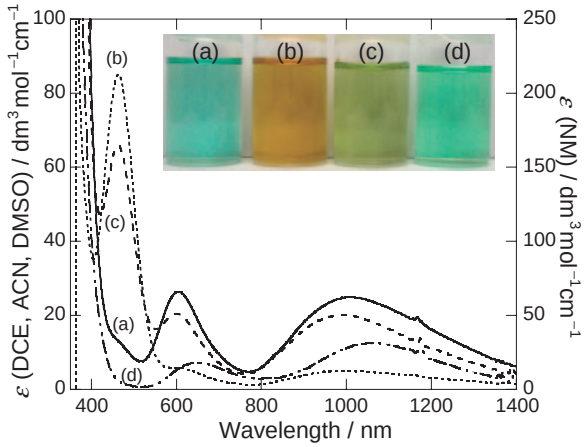

Fig. 9. UV–vis spectra of [Ni(acac)(dmap)NO_3] (**3**); (a) DCE, (b) NM, (c) ACN, and (d) DMSO. The peak at 1190 nm is due to noise from apparatus.

Table 6. Molar Conductivity ($ohm^{-1}\,cm^2\,mol^{-1}$ at 25 ± 0.1 °C)[a)]

Complex	DCE	NM	ACN	DMSO
2[b)]	22.3	85.3	131	20.1
3	1.34	26.6	29.7	18.8

a) Concentration of the complex is 0.00525 mol dm^{-3}. b) Taken as a 1:1 electrolyte reference value.

weaker bands corresponding to the octahedral species are also observed, as observed for the DCE solution (see Fig. 9). Thus, the weak donor NM does not coordinate to the Ni^{2+} ion. Therefore, the behavior of the complex in NM can be interpreted in terms of a shift of the equilibrium between Sp and Oh_1 species. In strong donor DMSO, the molar conductivity is almost the same as that of a 1:1 electrolyte and the spectrum is quite consistent with that of [Ni(acac)(dmap)]BF_4 in DMSO ([Ni(acac)(dmap)$(DMSO)_2$]$^+$) (Fig. 5c). It is considered that two solvent molecules replaced the NO_3^- from the complex and coordinated (Oh_2 structure). In ACN which has intermediate donor/acceptor properties, the molar conductivity shows that about 25 percent of the complex dissolved undergoes NO_3^- dissociation. However, the relative abundance ratio of the square-planar complex, estimated from the UV–vis spectrum, is much lower than 25 percent (ca. 10%) and the two bands attributable to the octahedral species correspond to neither those of complex **3** in DCE (Fig. 9a, Oh_1 structure) nor those of complex **2** in ACN (Fig. 5b, Oh_2 structure). These data suggest that there is an equilibrium among three structures; Sp, Oh_1, and Oh_2 in ACN solution. A possible reaction scheme of three complexes is illustrated in Fig. 10. For mixed-ligand nickel(II) systems containing the 1,3-diketonate and the diamine, their crystal structures with two solvent molecules show exclusively cis octahedral geometries.[24,25] However, in this study, there is a possibility of co-existence of cis and trans isomers in solution, and this point is remained as an open question.

Finally, when we compare the UV–vis spectra of the three square-planar nickel(II) complexes [Ni(acac)(L)]$^+$ (L = dmap in this work, dppe[10] and tmen[2]), it is noteworthy that the d–d transition band attributed to the square-planar structure shifts to higher energy with the increase in the number of the P-

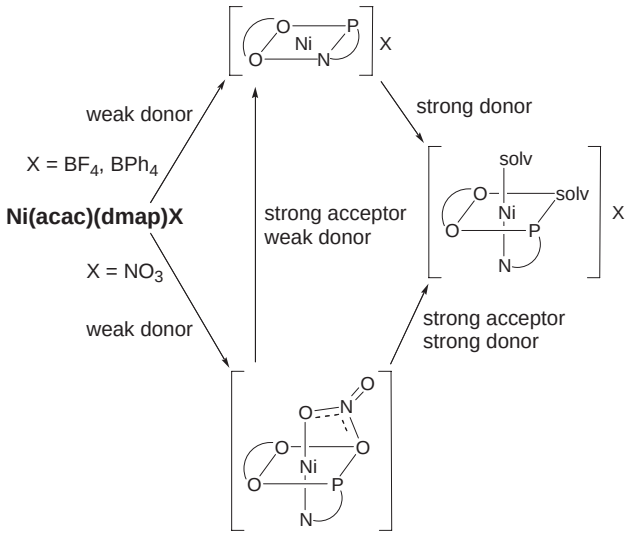

Fig. 10. Summary of the structures in solution. Only the cis isomer is illustrated for octahedral geometry.

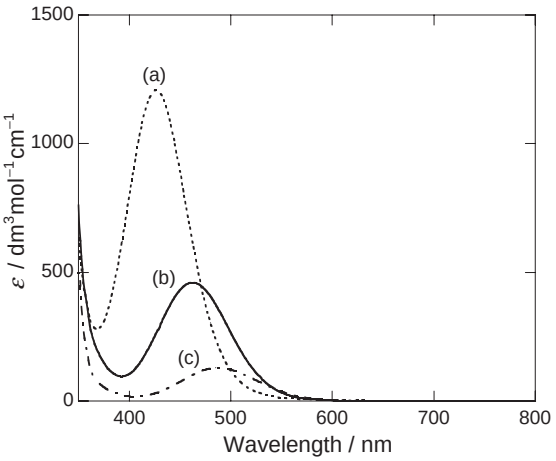

Fig. 11. UV–vis spectra of square-planar complexes, (a) [Ni(acac)(dppe)]BPh_4/dichloromethane, (b) [Ni(acac)-(dmap)]BPh_4/DCE, and (c) [Ni(acac)(tmen)]BPh_4/DCE.

donor atom bound to the Ni^{2+} ion; [Ni(acac)(tmen)]BPh_4 < [Ni(acac)(dmap)]BPh_4 < [Ni(acac)(dppe)]ClO_4 shown in Fig. 11. This result represents the order of the ligand field strength of the three ligands L. The stronger intensities in the d–d transition bands of the dmap and dppe complexes compared to the tmen complex arise from the covalent interaction between the soft phosphorus donor and the nickel(II) acceptor.

Conclusion

The structure of mixed-ligand complexes Ni(acac)(dmap)X (X = BPh_4, BF_4, and NO_3) in solid state varies by the donor strength of the anion X. In solution, these complexes showed solvatochromism and thermochromism depending on donor/acceptor properties of the solvent. The P-donor on the dmap ligand contributes to the stability of the square-planar structure of the complex when compared to the N-donor tmen complex. These results may be of importance in understanding the relationship between ligand field strength and chromotropism and of use in designing of new chromotropic complexes.

This work partly was supported by the Sasakawa Scientific Research Grant from The Japan Science Society (M.A.). The authors thank Prof. Yoichi Ishii, Chuo University, for his help with elemental analysis.

References

1 P. Gütlich, A. Hauser, S. Hartmut, *Angew. Chem., Int. Ed. Engl.* **1994**, *33*, 2024.

2 Y. Fukuda, K. Sone, *J. Inorg. Nucl. Chem.* **1972**, *34*, 2315; W. Linert, Y. Fukuda, A. Camard, *Coord. Chem. Rev.* **2001**, *218*, 113; K. Miyamoto, M. Sakamoto, C. Tanaka, E. Horn, Y. Fukuda, *Bull. Chem. Soc. Jpn.* **2005**, *78*, 1061.

3 A. Tamayo, J. Casabó, L. Escriche, C. Lodeiro, B. Covero, C. D. Brondino, R. Kivekäs, R. Sillampää, *Inorg. Chem.* **2006**, *45*, 1140.

4 K. Sone, Y. Fukuda, *Inorganic Thermochromism, Inorganic Chemistry Concept*, Springer, Heidelberg, **1987**, Vol. 10; N. Kimizuka, N. Oda, T. Kunitake, *Inorg. Chem.* **2000**, *39*, 2684.

5 M. Boiocchi, L. Fabbrizzi, F. Foti, M. Vázquez, *Dalton Trans.* **2004**, 2616.

6 J. Osugi, Y. Kitamura, *Nippon Kagaku Zasshi* **1968**, *89*, 569; K. Nakajima, M. Kojima, S. Azuma, R. Kasahara, M. Tsuchimoto, Y. Kubozono, H. Maeda, S. Kashino, S. Ohba, Y. Yoshikawa, J. Fujita, *Bull. Chem. Soc. Jpn.* **1996**, *69*, 3207.

7 Y. Fukuda, M. Hirota, M. Konno, A. Nakao, K. Umezawa, *Inorg. Chim. Acta* **2002**, *339*, 322; T. Hamaguchi, H. Nagino, K. Hoki, H. Kido, T. Yamaguchi, B. K. Breedlove, T. Ito, *Bull. Chem. Soc. Jpn.* **2005**, *78*, 591.

8 B. A. Prakasam, K. Ramalingam, M. Saravanan, G. Bocelli, A. Cantoni, *Polyhedron* **2004**, *23*, 77; C. C. Hadjikostas, H. H. Alkam, C. A. Bolos, P. C. Christidis, *Polyhedron* **2001**, *20*, 395.

9 G. Favero, B. Corain, M. Basato, S. Issa, *Inorg. Chim. Acta* **1986**, *122*, 129.

10 M. Arakawa, H. Miyamae, Y. Fukuda, *Bull. Chem. Soc. Jpn.* **2007**, *80*, 963.

11 V. Gutmann, *The Donor–Acceptor Approach to Molecular Interactions*, Plenum Press, New York, **1978**.

12 P. W. Selwood, *Magnetochemistry*, Interscience Publishers, New York, **1956**.

13 R. Malet, M. Moreno-Mañas, T. Parella, R. Pleixats, *J. Org. Chem.* **1996**, *61*, 758.

14 P. T. Beurskens, G. Admiraal, G. Beurskens, W. P. Bosman, S. Garcia-Granda, R. O. Gould, J. M. M. Smits, C. Smykalla, *PATTY: The DIRDIF Program System, Technical Report of the Crystallography Laboratory*, University of Nijmengen, The Netherlands, **1992**.

15 P. T. Beurskens, G. Admiraal, G. Beurskens, W. P. Bosman, R. de Gelder, R. Israel, J. M. M. Smits, *DIRDIF99: The DIRDIF-99 Program System, Technical Report of the Crystallography Laboratory*, University of Nijmengen, The Netherlands, **1999**.

16 *CrystalStructure 3.7.0, Crystal Structure Analysis Package*, Rigaku and Rigaku/MSC, **2000–2005**; D. J. Watkin, C. K. Prout, J. R. Carruthers, P. W. Betteridge, *CRYSTALS Issue 10*, Chemical Crystallography Laboratory, Oxford, UK, **1996**.

17 G. M. Sheldeick, *SHELXS97, Program for the Refinement of Crystal Structures*, University of Göttingen, Germany, **1997**.

18 A. Altomare, G. Cascarano, C. Giacovazzo, A. Guagliardi, M. C. Burla, G. Polidori, M. Camalli, *J. Appl. Crystallogr.* **1994**, *27*, 435.

19 *SADABS: Sub-program of SAINT-plus*, Siemans, Siemans Analytical X-rays Instrument Inc., Madison, Wisconsin, USA, **1995**.

20 *teXsan: Crystal Structure Analysis Package*, Molecular Structure Corporation, **1985** and **1999**.

21 S. Yamada, *Coord. Chem. Rev.* **1966**, *1*, 415; A. B. P. Lever, *Inorganic Electronic Spectroscopy: Studies in Physical and Theoretical Chemistry*, Elsevier, Amsterdam, **1984**, Vol. 33.

22 A. B. P. Lever, E. Montovani, B. S. Ramaswamy, *Can. J. Chem.* **1971**, *49*, 1957.

23 Y. Fukuda, C. Fujita, H. Miyamae, H. Nakagawa, K. Sone, *Bull. Chem. Soc. Jpn.* **1989**, *62*, 745.

24 F. Murata, M. Arakawa, A. Nakao, K. Satoh, Y. Fukuda, *Polyhedron* **2007**, *26*, 1570.

25 K. Yamada, K. Hori, Y. Fukuda, *Acta Crystallogr., Sect. C* **1993**, *49*, 445.